1

Supplementary Information for

Compressed vessels bias red blood cell partitioning at bifurcations in a hematocrit-dependent manner: implications in tumor blood flow

Romain Enjalbert, David Hardman, Timm Krüger and Miguel O. Bernabeu

Timm Krüger and Miguel O. Bernabeu.

E-mail: timm.krueger@ed.ac.uk, miguel.bernabeu@ed.ac.uk

This PDF file includes:

Supporting Information Text

The supplementary information text contains additional details of the model for particulate blood flow.

Details of the numerical methods

In the following, the numerical model for red blood cells (RBCs) suspended in blood plasma is summarised. The model has been shown to recover the most important properties of red blood cell flow relevant to this study, *i.e.* the motion and deformation of individual RBCs and dense suspensions of RBCs (1, 2), and the partitioning of RBCs in a semi-dilute suspension within a network (3). The interested reader is referred to (4, 5) for more details about the method.

Fluid model.. The lattice-Boltzmann method (LBM) is used to numerically solve the Navier-Stokes equation for our Newtonian fluid model; see (6) for more details on the LBM. Our LBM algorithm employs the D3Q19 lattice, the Bhatnagar-Gross-Krook collision operator, Guo's forcing scheme (7), the Bouzidi-Firdaouss-Lallemand no-slip boundary condition at the walls (8), and the Ladd velocity boundary condition for inlets/outlets (9). The parameters for the LBM are provided in Table S1.

Red blood cell model.. Each RBC is modelled as a biconcave discocyte with shape parameters taken from physiological RBCs (10). The RBC model includes a membrane energy,

$$W = W^S + W^B + W^A + W^V, \tag{1}$$

where each superscript S, B, A, V denotes the source of the energy contribution, strain, bending, area and volume energies, respectively. Our model uses the surface strain energy density for RBCs as proposed by Skalak et al. (11),

$$W^S = \oint w^S \, dA, \quad w^S = \frac{\kappa_s}{12}(I_1^2 + 2I_1 - 2I_2) + \frac{\kappa_\alpha}{12}I_2^2, \tag{2}$$

where κ_s and κ_α are the elastic shear and dilation moduli. κ_s is set through the capillary number and κ_α is set to maintain near incompressibility of the RBC membrane. I_1 and I_2 can be calculated from the local stretch ratios; see (5) for details. The strain energy W^S is discretised as

$$W^S = \sum_{j=1}^{N_f} A_j^{(0)} w_j^S, \tag{3}$$

where each RBC membrane is approximated by a mesh of N_f triangular faces j of initial undeformed area $A_j^{(0)}$. The remaining three energy contributions (bending, surface area, volume) are calculated through

$$W^B = \sqrt{3}\kappa_B \sum_{\langle i,j \rangle} (\theta_{i,j} - \theta_{i,j}^{(0)})^2, \tag{4}$$

where $\theta_{i,j}$ is the angle between two neighbouring triangular faces,

$$W^A = \frac{\kappa_A(A - A^{(0)})^2}{2A^{(0)}}, \tag{5}$$

where A is the surface area of the RBC,

$$W^V = \frac{\kappa_V(V - V^{(0)})^2}{2V^{(0)}}. \tag{6}$$

where V is the volume of the RBC. The superscript (0) denotes values for an undeformed RBC. κ_B, κ_A, κ_V are the bending, surface area and volume moduli. κ_B is known from experiments, whereas κ_A and κ_V are set to achieve conservation of the surface area and volume of each RBC (4, 5). The forces acting on each vortex of an RBC mesh are calculated through the principle of virtual work:

$$\vec{F}_i = -\frac{\delta W}{\delta \vec{x}_i}, \tag{7}$$

where $\vec{F}_i$ is the force acting on the ith node, W is the total energy functional, and $\vec{x}_i$ is the position of the node. The parameters for the RBC model are provided in Table S2.

Fluid-cell interaction.. The RBC membrane is coupled to the fluid through the immersed boundary method (IBM) (4). After the forces acting on each vortex of the mesh of an RBC have been calculated, these forces are spread to the fluid lattice:

$$\vec{f}(\vec{X}, t) = \sum_i \vec{F}_i(t)\delta(\vec{X} - \vec{x}_i(t)), \tag{8}$$

where $\vec{f}(\vec{X}, t)$ is the force density acting on the fluid node at position $\vec{X}$ and time t, $\vec{F}_i(t)$ is the force acting on the ith membrane node, and $\delta(\vec{X} - \vec{x}_i(t))$ is a discretised delta function. We use a three-point stencil for the discretised delta function (4). The force that is spread from the RBC mesh to the fluid lattice is considered as external force during the next lattice-Boltzmann

Romain Enjalbert, David Hardman, Timm Krüger and Miguel O. Bernabeu

time step. Once the flow field has been updated at time $t + \Delta t$ through the LBM, the fluid velocity is interpolated at each RBC mesh vortex:

$$\vec{u}_i(t + \Delta t) = \sum_{\vec{X}} \vec{u}(\vec{X}, t + \Delta t)\delta(\vec{X} - \vec{x}_i(t)), \qquad [9]$$

where $\vec{u}_i(t + \Delta t)$ is the velocity of the ith RBC mesh node at time $t + \Delta t$ and $\vec{u}(\vec{X}, t + \Delta t)$ is the updated velocity at a fluid lattice point $\vec{X}$. RBC mesh vortices are updated according to

$$\vec{x}_i(t + \Delta t) = \vec{x}_i(t) + \vec{u}_i(t + \Delta t)\Delta t, \qquad [10]$$

and the overall algorithm proceeds to the next iteration.

**Table S1. Simulation parameters used for the lattice-Boltzmann method.**

Parameter	Symbol	Unit	Value
Voxel size	Δx	μm	0.6667
Timestep	Δt	s	7.41×10^{-8}
Relaxation time	τ	dimensionless	1
Fluid viscosity	μ	mPa s	1
RBC cytoplasm viscosity	μ	mPa s	1
Fluid density	ρ	kg/m^3	1000

Table S2. Parameters used for the red blood cell model. All values are given in simulation units, unless specified otherwise.

Parameter	Symbol	Value
Strain modulus	κ_s	depends on capillary number
Dilation modulus	κ_α	0.5
Bending modulus	κ_B	depends on capillary number
Surface area modulus	κ_A	1
Volume modulus	κ_V	1
Föppl-von Kármán number	$\Gamma = \kappa_B/(\kappa_S r_{RBC}^2)$	1/400
Number of faces in RBC mesh	N_f	720
RBC radius	r_{RBC}	4 μm
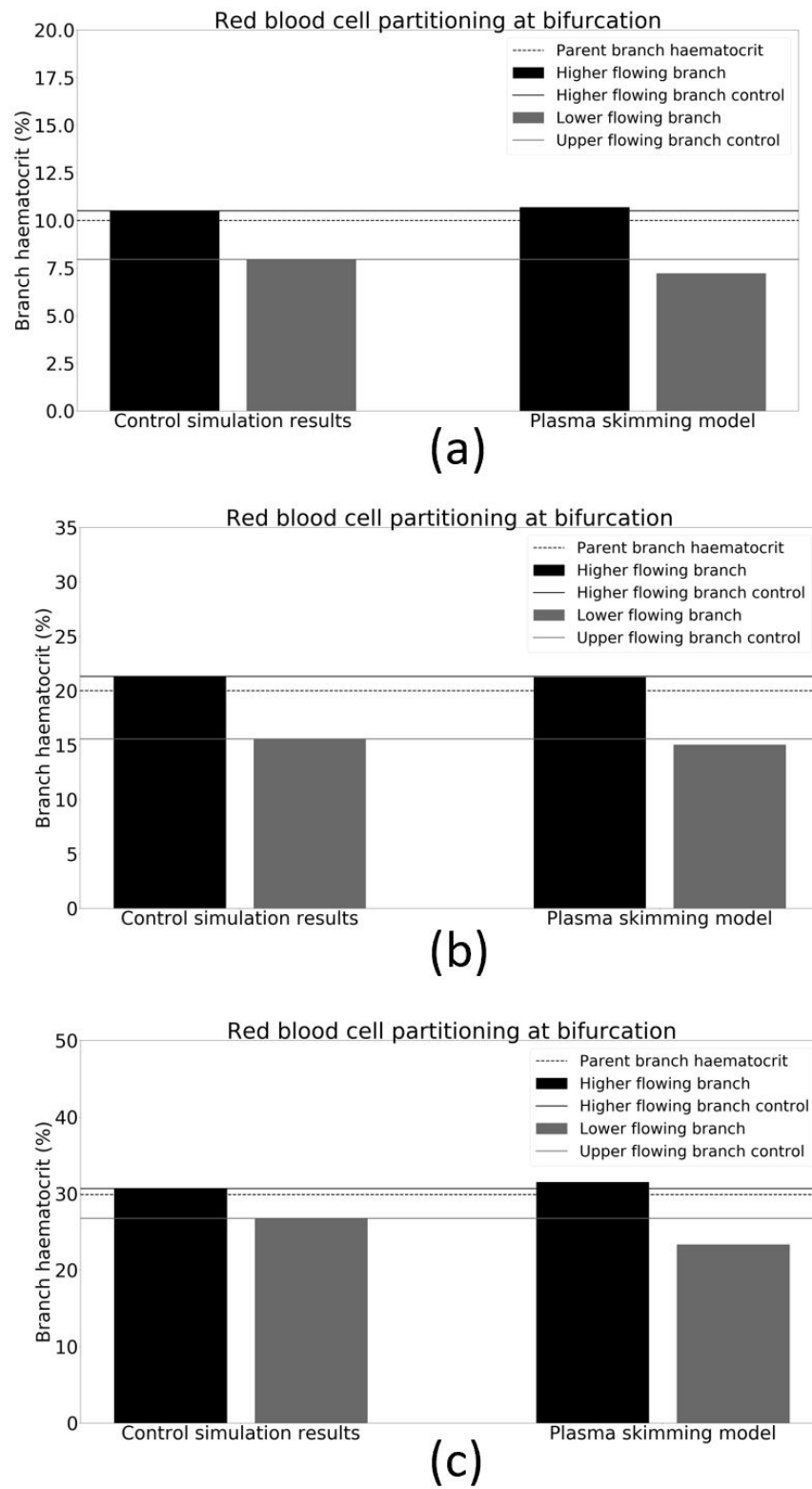
Fig. S1. Comparison of simulation control data with empirical plasma skimming model ([12](), [13]()) with a flow ratio of 4. (a) Simulation at $H_d = 10\%$. (b) Simulation at $H_d = 20\%$. (c) Simulation at $H_d = 30\%$.

**Romain Enjalbert, David Hardman, Timm Krüger and Miguel O. Bernabeu**
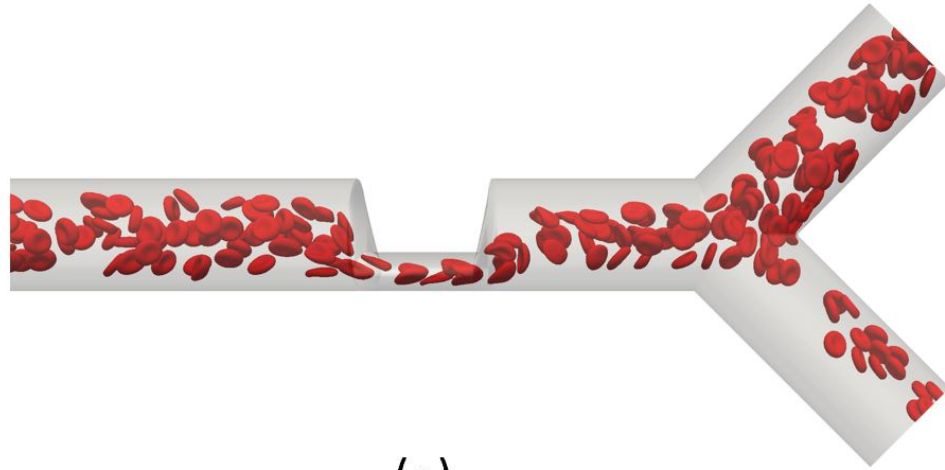
(a)
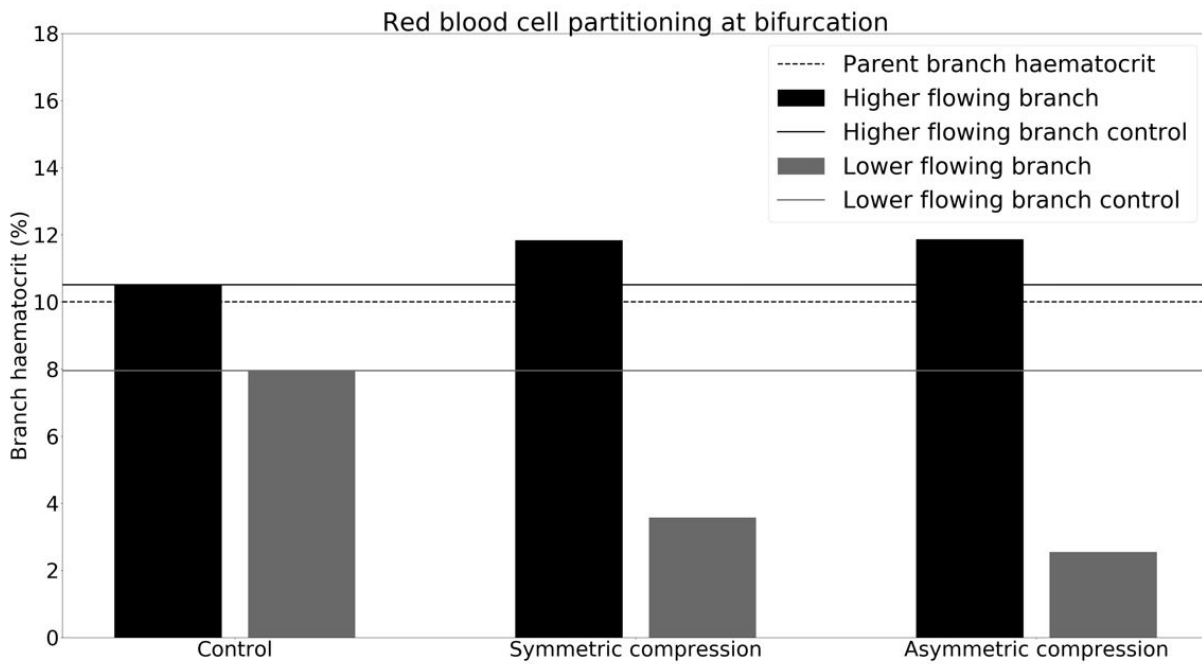
(b)

Fig. S2. Phase separation of child branches after bifurcation at $H_d = 10\%$ comparing effect of compression asymmetry. (a) Snapshot of the asymmetric short geometry with the same dimensions as the short geometry. (b) From left to right are the hematocrit of the child branches for a control geometry, a symmetric compression, and an asymmetric compression (a). Results show a negligible difference between a symmetric and asymmetric geometry. In black is the higher flowing child branch and in grey the lower flowing child branch. The solid lines are the control discharge hematocrits. The dotted line illustrates the discharge hematocrit of the parent branch.
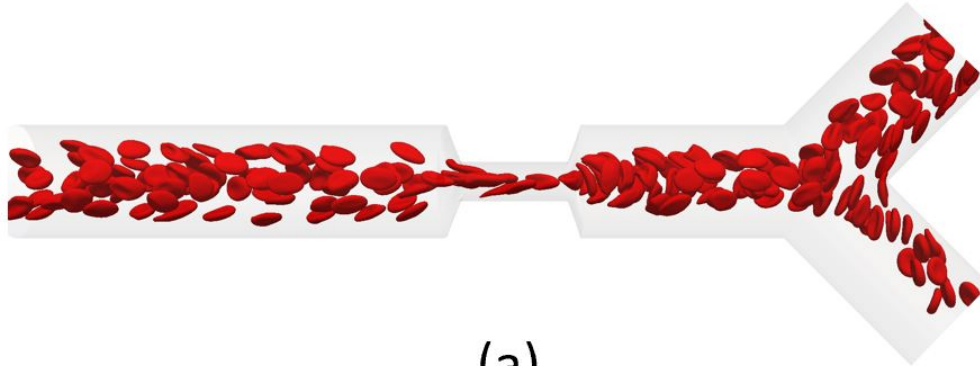
(a)
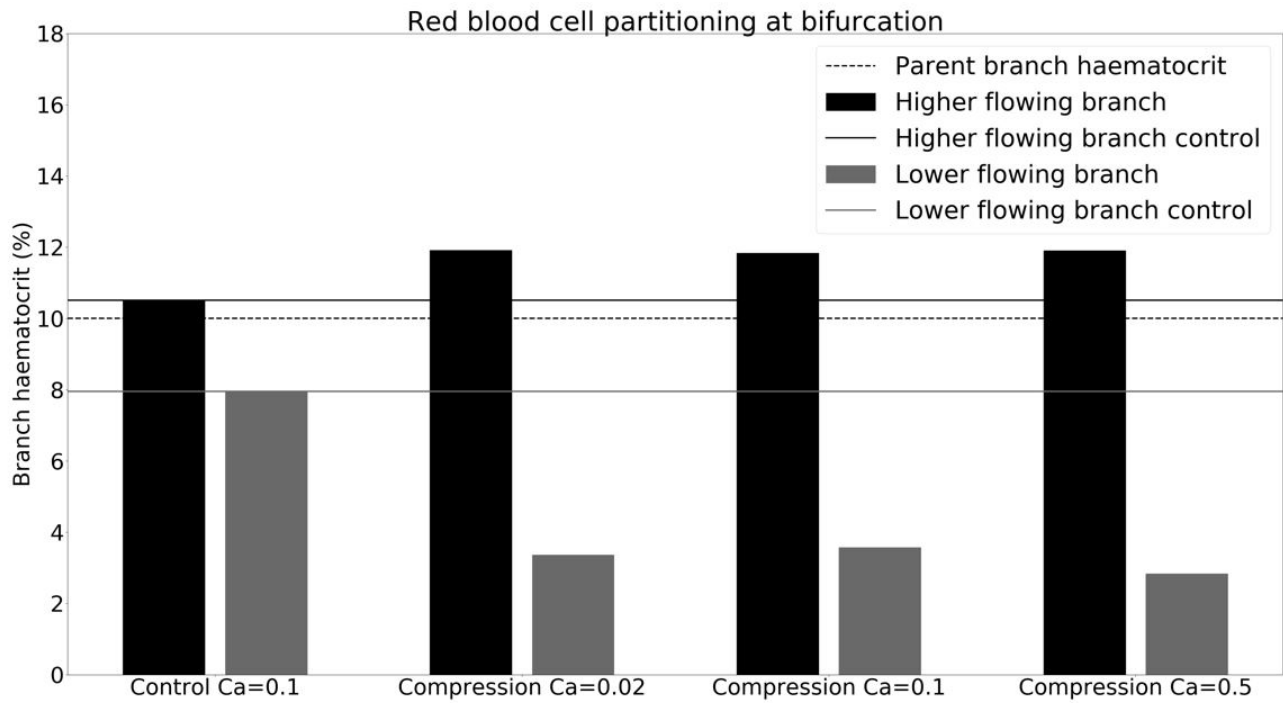
(b)

Fig. S3. Phase separation of child branches after bifurcation at $H_d = 10\%$, comparing effect of different channel flow rates (increasing capillary number denotes increasing flow rate). (a) Snapshot of the short compression with a higher channel flow rate and a capillary number of 0.5. (b) hematocrit of the child branches for a control geometry, on the left, and a compression geometry (a) at three different capillary numbers. In black is the higher flowing child branch and in grey the lower flowing child branch. The solid lines are the control discharge hematocrits. The dotted line illustrates the discharge hematocrit of the parent branch.
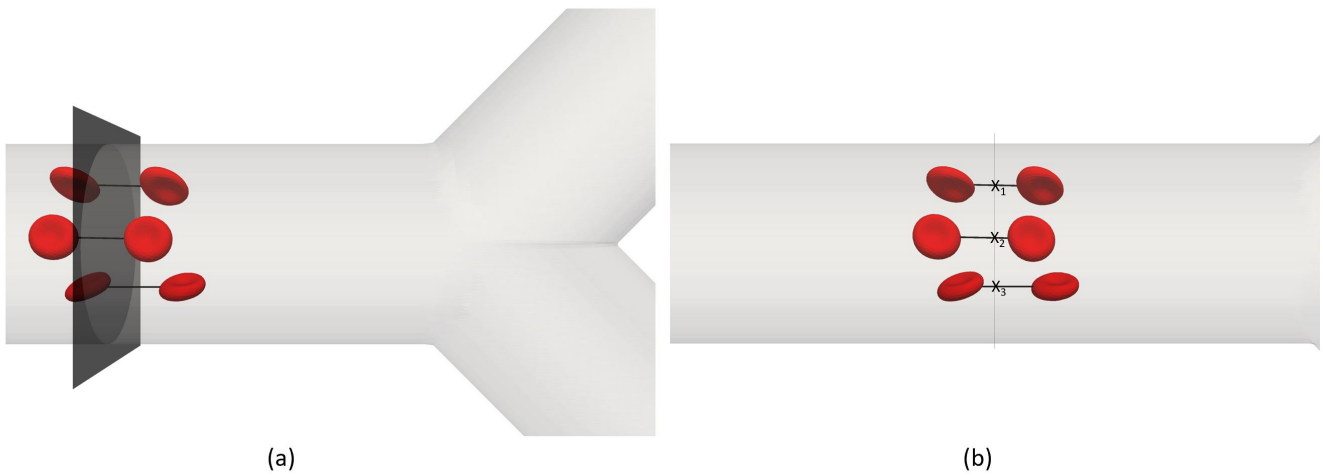
Romain Enjalbert, David Hardman, Timm Krüger and Miguel O. Bernabeu

(a)   (b)

Fig. S4. (a) Three RBCs before and after a plane of interest. Lines indicate RBC trajectories, assumed as straight. (b) Side view as each cell crosses the plane at a given coordinate (x, y, z). The RMSD is calculated in the compression axis (here seen as height of channel) by setting x_0 as the channel centreline (always zero) and x_i as the height coordinate of the RBC as it crosses the plane. This measures the distribution in the height of the channel. For illustration purposes only three cells are shown, whereas several hundred are accounted for.
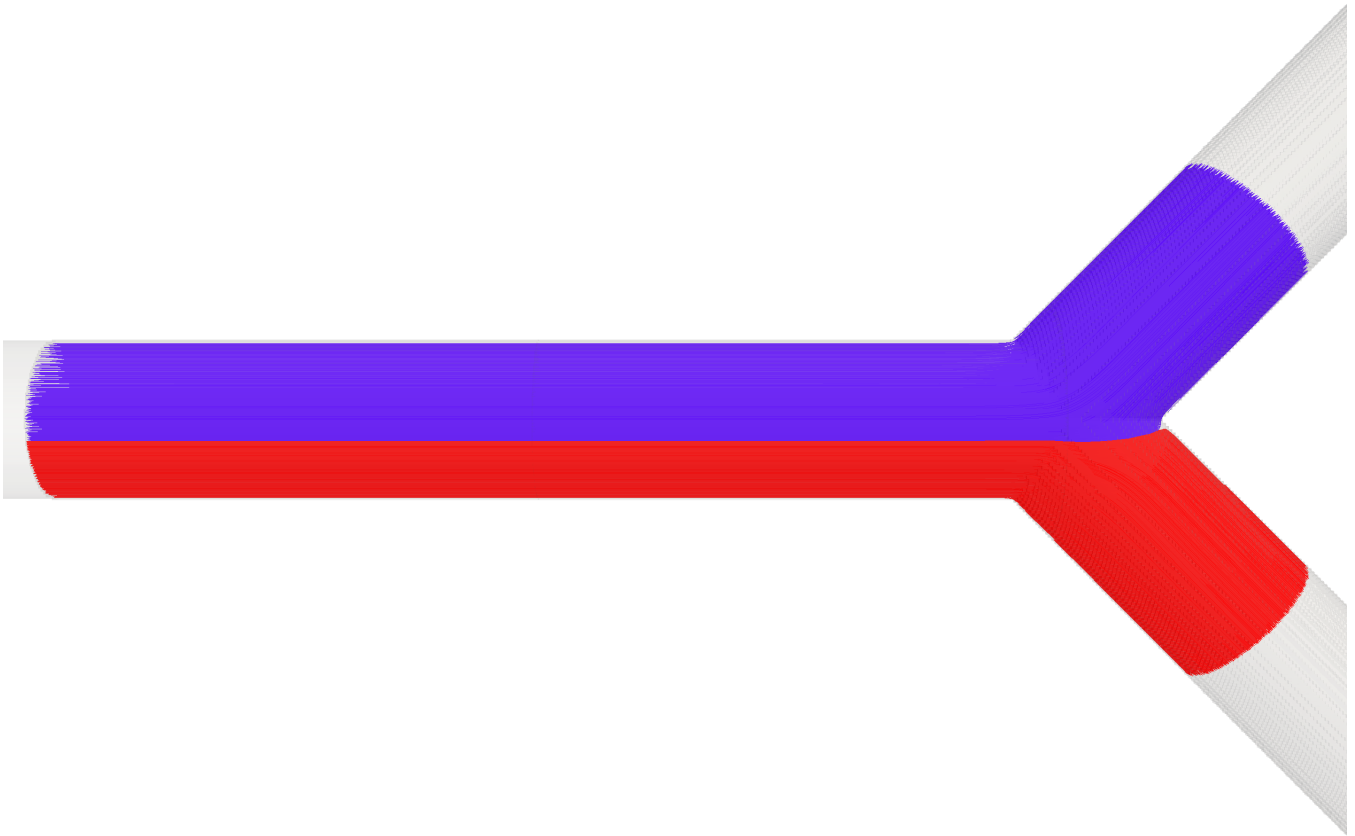
Fig. S5. Intuition for separatrix. Blue/red lines are streamlines ending in the top/bottom child branch, respectively. The separatrix is the surface separating the blue from the red streamlines on the plane.

Romain Enjalbert, David Hardman, Timm Krüger and Miguel O. Bernabeu

References

1. T Krueger, margination and near-wall dynamics. *Rheol. Acta* (2015).
2. T Krüger, D Holmes, PV Coveney, Deformability-based red blood cell separation in deterministic lateral displacement devices-A simulation study. *Biomicrofluidics* **8** (2014).
3. Q Zhou, J Fidalgo, MO Bernabeu, MSN Oliveira, T Krüger, Emergent cell-free layer asymmetry and biased haematocrit partition in a biomimetic vascular network of successive bifurcations. *Soft Matter* (2021).
4. T Krüger, F Varnik, D Raabe, Efficient and accurate simulations of deformable particles immersed in a fluid using a combined immersed boundary lattice Boltzmann finite element method. *Comput. Math. with Appl.* **61**, 3485–3505 (2011).
5. Timm Krüger, Ph.D. thesis (2012).
6. T Kruger, et al., *The lattice boltzmann method, principles and practice.* (Springer) No. 207, pp. 1–705 (2017).
7. Z Guo, C Zheng, B Shi, Discrete lattice effects on the forcing term in the lattice Boltzmann method. *Phys. Rev. E - Stat. Physics, Plasmas, Fluids, Relat. Interdiscip. Top.* **65**, 1–6 (2002).
8. M Bouzidi, M Firdaouss, P Lallemand, Momentum transfer of a Boltzmann-lattice fluid with boundaries. *Phys. Fluids* **13**, 3452–3459 (2001).
9. AJ Ladd, Numerical Simulations of Particulate Suspensions Via a Discretized Boltzmann Equation. Part 1. Theoretical Foundation. *J. Fluid Mech.* **271**, 285–309 (1994).
10. E Evans, YC Fung, Improved Measurements of the Erythrocyte Geometry. *Microvasc. research* **4**, 335–347 (1972).
11. R Skalak, A Tozeren, RP Zarda, S Chien, Strain Energy Function of Red Blood Cell Membranes. *Biophys. J.* **13**, 245–264 (1973).
12. A Pries, K Ley, M Classen, P Gaehtgens, Red Cell Distribution at Microvascular. *Microvasc. research* **38**, 81–101 (1989).
13. AR Pries, TW Secomb, Microvascular blood viscosity in vivo and the endothelial surface layer. *Am. J. Physiol. - Hear. Circ. Physiol.* **289**, 2657–2664 (2005).